Food Chemistry: X 22 (2024) 101377

Contents lists available at ScienceDirect

Food Chemistry: X

journal homepage: www.sciencedirect.com/journal/food-chemistry-x

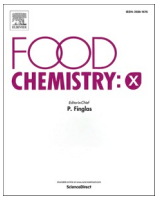

Construction of emulsion gel based on the interaction of anionic polysaccharide and soy protein isolate: Focusing on structural, emulsification and functional properties

Tian Gao, Xixi Wu, Yiting Gao, Fei Teng *, Yang Li *

College of Food Science, Northeast Agricultural University, Harbin, Heilongjiang 150030, China

ARTICLE INFO

Keywords:
Soybean protein isolate
Anionic polysaccharides
Emulsion gels
Structure
Functional properties

ABSTRACT

In this study, the effects on the structures and emulsion gels of carrageenan (CA) and gum arabic (GA) with soybean protein isolate (SPI) were investigated. The results showed that CA and GA exposed hydrophobic groups to SPI, and formed complexes through non-covalent interactions to improve the stability of the complexes. Furthermore, the emulsion gels based on the emulsions exhibited that CA formed emulsion-filled gels with higher elasticity, stronger gel strength, and thermal reversibility, whereas GA formed emulsion-aggregated gels with higher viscosity, and a weak-gel network. The results of digestion showed that, CA was more helpful to slow down the release of free fatty acids and protect vitamin E during digestion. Compared with SPI-GA emulsion gel, SPI-CA emulsion gel had better physicochemical properties and stronger network structure. The results of this study may be useful in the development of anionic polysaccharides that interact with SPI, and they may provide new insights on the preparation of emulsion gels that slowly release fat-soluble nutrients.

1. Introduction

Soybean protein isolate (SPI) is a commercial plant protein ingredient with high quality (C. Chen, Sun-Waterhouse, Zhang, Zhao, & Sun, 2020). Its molecular characteristics give it both hydrophilic and lipophilic properties, so it can be adsorbed at the oil-water interface to maintain the stability of the disperse phase (Qingyun Li, Zheng, Ge, Zhao, & Sun, 2020). SPI is also a common emulsifier for preparing emulsions, with high nutritional value and low production cost. It is widely used in the preparation of emulsions and gels as well as the transport of bioactive components. However, native SPI is prone to form aggregates in polar environments due to its poor solubility and it is sensitive to the changes in the environment, which seriously limits its application (Puppo et al., 2008). To solve this problem, it is important to develop green, efficient, and low-cost protein modification methods to alter the structure of SPI so as to improve its utilization. Polysaccharides have excellent physicochemical properties and are widely used by researchers to improve the functional properties of proteins. Loyeau, Spotti, Vinderola, and Carrara (2021) used whey protein isolate/dextran conjugate by Maillard reaction as emulsifier to prepare emulsion with smaller oil droplets, better stability, and higher encapsulation efficiency for probiotic bacteria. Li et al. (2021) prepared W/O/W emulsion through the complex of soybean lipophilic protein and methyl cellulose, which improved the viscoelasticity and the encapsulation efficiency of vitamin B_{12}.

Carrageenan (CA) is a water-soluble and straight-chain polysaccharide extracted from Rhodophyta with sulfate groups attached to galactose, CA has net negative charge and it has good stability, biocompatibility, and gelation, and it is environmentally friendly (Guo et al., 2022). Gum Arabic (GA), an anionic polysaccharide extracted from the natural exudates of Acacia, has carboxyl groups attached to glucuronic acid residues, and it carries a negative charge at pH values >2.2. In addition, GA is highly water-soluble and environmentally friendly, and it has excellent gelation and film-forming ability. Two kinds of anionic polysaccharides, CA and GA, which can form complexes with SPI through electrostatic interactions, can effectively improve the solubility of SPI and enhance its properties. Therefore, CA and GA have excellent physicochemical properties and are widely used in the food industry, and are superior raw materials for improving the stability and properties of emulsion gels. Liu, Zhao, Hu, and Lin (2003) found that Kappa carrageenan interacted with SPI to form emulsion gel by electrostatic attraction, which significantly improved gel textural and rheological properties. Gali, Bedjou, Ferrari, and Donsi (2022) embedded rutin in zein nanoparticles stabilized by GA, the electrostatic

* Corresponding authors.
E-mail addresses: tengfei@neau.edu.cn (F. Teng), yangli@neau.edu.cn (Y. Li).

https://doi.org/10.1016/j.fochx.2024.101377
Received 15 September 2023; Received in revised form 7 April 2024; Accepted 9 April 2024
Available online 10 April 2024

interaction between zein and GA significantly enhanced the stability of zein nanoparticles and the encapsulation efficiency of rutin.

Emulsion gels have properties of both emulsions and gels. They have high stability and are easy to store and transport, and are therefore commonly used as sustained-release carriers for active components. Moreover, emulsion gels can be added to food products as fat substitutes, which reduces the fat content of certain foods. Proteins and polysaccharides are often used to form a matrix in emulsion gels, but their application is limited due to the unstable properties of native proteins or polysaccharides, hence modification by physical, chemical, and biological methods not only improve the stability but also improve the physicochemical and functional characteristics of products prepared by proteins and polysaccharides. Khalesi, Emadzadeh, Kadkhodaee, and Fang (2019) studied the influence of Persian gum on concentrated whey protein emulsion gels by salt induction, and they found that the addition of Persian gum could improve the viscoelasticity and microstructure of the gel. Zhang et al. (2021) evaluated the effects of binding degree of whey protein and flaxseed gum on emulsion gel with embedded astaxanthin, and the study showed that the emulsion gel had higher grafting degree and more expanded structures, and the water holding capacity, encapsulation efficiency, and stability of the emulsion gel were improved. Presently, there are few studies on the complexes prepared by anionic polysaccharides and SPI, and few studies compare the effects of two polysaccharides on the stability of SPI emulsion gels.

This study aimed to utilize CA and GA to modify SPI to form complexes, and to prepare the emulsion gels by using SPI-CA and SPI-GA complexes. Through the characterization of the complexes and the emulsion gels, the effects of two anionic polysaccharides on SPI structure and the emulsion gels were compared. In addition, digestion behavior in vitro showed that the effects of the emulsion gels on slowing down the release of active substances. This study enriches the preparation methods of SPI emulsion gel and provides a theoretical basis for the development of bioactive substance delivery systems.

2. Materials and methods

2.1. Materials

SPI (protein 90.13%, *w*/w) was supplied by Yousuo Chemical Technology Co., Ltd. (Shandong, China). Corn oil was obtained from a local market (Harbin, China). Carrageenan (CAS#9000-07-1, intensity 1200), gum arabic, and vitamin E were purchased from Yuanye Biotechnology Co., Ltd. (Shanghai, China). Distilled water was used, and all other chemicals used in the study were of analytical grade.

2.2. Preparation of complexes and emulsion gels

2.2.1. Complexes preparation

SPI and anionic polysaccharides were prepared as dispersion and solution of certain concentrations, respectively. In brief, polysaccharide solutions of 0.01%, 0.05%, 0.10%, and 0.20% (*w*/w) were combined with the SPI dispersion to prepare a SPI dispersion of 5.00%, followed by adjusting the pH of the solution to 7.00 ± 0.02 with 1 M NaOH or 1 M HCl and stirring at room temperature for 1 h to allow the solution to fully react. SPI, as the control, and the complexes prepared by SPI with polysaccharide concentrations of 0.01%, 0.05%, 0.10%, and 0.20% (*w*/w) were named SPI, CA1/GA1, CA2/GA2, CA3/GA3, and CA4/GA4 respectively. The emulsions and emulsion gels were named in the same way.

2.2.2. Emulsion gels preparation

Corn oil (20.0%, *v*/v) was added to the solution, dispersed at high speed at 1000 rpm for 3 min with the ULTRA-TURRAX disperser (IKA, Staufen, Germany), and homogenized at 80 MPa two times to obtain the emulsions. Vitamin E (1.00%, v/v) was added to the corn oil and stirred at 600 rpm for 30 min at room temperature to evenly disperse the vitamin E in the corn oil to prepare the emulsions for the analysis of digestion characteristics.

The emulsions were heated at 90 °C for 30 min in a water bath and cooled to room temperature. Next, 30 mmol $CaCl_2$ was added to the emulsions, followed by mixing. The samples were heated at 85 °C for 15 min in a water bath, cooled to room temperature quickly, stored in a refrigerator at 4 °C, and analyzed after the emulsion gels were formed.

2.3. SPI-CA/GA complex characterization

2.3.1. Fourier transform infrared spectroscopy (FT-IR)

The secondary structures of the complexes were measured with the Nicolet is50 Fourier transform infrared spectrometer (Thermo Fisher Scientific, Waltham, USA). In brief, 2 mg of the dried samples were mixed with 100 mg of the potassium bromide solid according to certain proportions, ground and pressed into a tablet, and measured. The temperature was set to 25 °C, the scanning wave number ranged from 4000 to 400 cm^{-1}, the wave number accuracy was 0.005 cm^{-1}, and scanning was performed 64 times.

2.3.2. Intrinsic fluorescence spectrum

The method of Ma et al. (2020) was slightly modified, and the samples prepared in **Section 2.2.1** were diluted 100 times with distilled water. Next, the excitation wavelength was set to 295 nm and the slit was set to 5 nm, followed by the scanning of the control fluorescence spectrum with an emission wavelength range of 300–400 nm at 25 °C.

2.3.3. Particle size and zeta potential

The particle size and Zeta potential were evaluated by dynamic light scattering (DLS). After the samples were diluted 100 times with distilled water, the refractive index of the aqueous phase was set to 1.33 at 25 °C and measured at a fixed detection angle of 90° (Zhao et al., 2022).

2.3.4. Surface hydrophobicity (H_0)

The surface hydrophobicity of the complexes was determined with the 1-anilino-8-naphthalene sulfonate (ANS) fluorescent probe method (Lee et al., 2016). In brief, 0.01 mol/L phosphate buffer saline with pH 7.00 ± 0.02 was prepared, and this solution was used to prepare the ANS stock solution with a concentration of 8 mmol. The samples were diluted to prepare five concentrations ranging from 0.02 to 0.10 mg/mL. After adding 100 μL of the ANS solution to the diluted sample (10 mL) in darkness, the fluorescence intensity was measured with the F-4500 fluorescence spectrophotometer (Hitachi, Tokyo, Japan) after mixing. The excitation wavelength was set to 340 nm, and the emission wavelength was set to 440 nm. The initial slope of the fluorescence intensity and the protein concentration were represented as the surface hydrophobicity value of the SPI sample.

2.3.5. Emulsification properties

The emulsification properties were measured according to the method of Josaé et al. (Lopes-da-Silva & Monteiro, 2019) and it was slightly modified, the analysis was conducted with the UV-2600 ultraviolet-visible spectrophotometer (Shimadzu, Kyoto, Japan). In brief, the emulsions in **Section 2.2.2** were diluted 1000 times (*v*/v) with 0.1% SDS solution, and the absorbance values (A_0) were measured at 500 nm. The emulsions were left undisturbed for 30 min, and the absorbance values (A_{30}) were measured again. The emulsifying activity index (EAI) and the emulsifying stability index (ESI) were measured according to the following formula:

$$\mathrm{EAI}\left(\frac{\mathrm{m}^2}{\mathrm{g}}\right) = 2 \times 2.303 \frac{\mathrm{A}_0 \times \mathrm{D}_\mathrm{F}}{\mathrm{c} \times \phi \times (1-\theta) \times 10000} \approx 65.8 \times \mathrm{A}_0 \quad (1)$$

$$\mathrm{ESI}(min) = \frac{\mathrm{A}_0}{\mathrm{A}_0 - \mathrm{A}_{30}} \times 30 \quad (2)$$

Where A_0 represents the absorbance values at 0 min (500 nm), A_{30}

represents the absorbance values at 30 min (500 nm), D_F is the dilution factor (1000), C is the initial protein concentration (1.00 g/100 mL), ϕ is the optical path (0.01 m), and θ is the fraction of the oil phase (0.20).

2.4. SPI-CA/GA emulsion gel characterization

2.4.1. Scanning electron microscope (SEM)

The S-3400 N scanning electron microscope (Hitachi, Tokyo, Japan) was used to characterize the microstructure of the gels (Li et al., 2021). The emulsion gels were cut into 2 mm squares, and the samples were fixed in glutaraldehyde solution pH 6.8 for >6 h at 4 °C and rinsed three times in phosphate buffer saline pH 6.8. The rinsed samples were subjected to gradient elution with ethanol solutions (ethanol concentrations of 50%, 70%, 90%, and 100%) for 10 min each, and the samples were stored in a refrigerator at −20 °C for 30 min after t-butanol replacement and stored in a freezer for drying. Next, the dried samples were stuck to conductive tape and placed on a sample table. The samples were coated with a layer of metal film with an ion sputter coater, and after gold spraying, the microstructure of the emulsion gels was observed under a scanning electron microscope with a magnification of ×3000.

2.4.2. Determination of the force of emulsion gels

The force of the emulsion gels during gel formation was reflected by the solubility of the emulsion gels in different solvents as follows: the different structures were broken by stepwise dissolution, and the magnitude of the force was reflected by the protein content to the total protein content in each solvent. The S1 (0.6 mol/L NaCl) solvent could break ionic bonds; the S2 (a mixture of 1.5 mol/L urea and 0.6 mol/L NaCl) mixed solvent could break ionic and hydrogen bonds; the S3 (a mixture of 8 mol/L urea and 0.6 mol/L NaCl) mixed solvent could break ionic bonds, hydrogen bonds, and hydrophobic interactions; the S4 (0.5 mol/L β-mercaptoethanol, 8 mol/L urea, and 0.6 mol/L NaCl, pH 7.00) mixed solvent could break ionic bonds, hydrogen bonds, hydrophobic interactions, and disulfide bonds. Next, 5 ml of each sample was added to 10 mL of S1 solution and centrifuged at 10000 *g* for 10 min to obtain the precipitate and the supernatant, and 10 mL of S2 solution was added to the precipitate and centrifuged at 10000 *g* for 10 min to obtain the precipitate. S3 and S4 solution used the same steps. Lastly, 2 mL of 1 mol/L NaOH solution was added to the final precipitate, which was dissolved and centrifuged at 5000 *g* for 10 min to obtain the supernatant. The protein content in all supernatants was determined with the Coomassie brilliant blue method.

2.4.3. Water holding capacity

The water holding capacity of the emulsion gels was determined according to the method of Anne et al. (Maltais, Remondetto, Gonzalez, & Subirade, 2005). The emulsion gels were weighed in centrifuge tubes and centrifuged at 10000 *g* for 30 min. The water released from the gels was removed after centrifugation, and the remaining emulsion gels were weighed. The water holding capacity (WHC) of the emulsion gels was calculated according to the following formula:

$$\mathrm{WHC} = \frac{\mathrm{Wt} - \mathrm{Wr}}{\mathrm{Wt}} \times 100\% \tag{3}$$

Where W_t is the total mass of the sample, and W_r is the mass contained in the gel.

2.4.4. Texture measurement

The texture was assessed to reflect the mechanical properties of the emulsion gels. The textural properties of the emulsion gels were determined by the plus-10,704 extrusion instrument (LOTUN, Shanghai, China) with a probe of P/0.5. The speed was constant at 1.00 mm/s before the test, the test speed and the speed after the test were constant at 5 mm/s, the stress was constant at 3 g, and the test distance was 50% of the height of the emulsion gels. The hardness, viscoelasticity, cohesion, and chewiness of the samples were recorded (Li, Liu, et al., 2021). All the tests were performed at room temperature.

2.4.5. Rheological behavior

Rheological behavior was measured by RST-CPS rheometer (Brookfield, Massachusetts, USA) according to Kornet et al. (2022). The emulsions in **Section 2.2.2** were placed between two parallel plates (diameter, 50 mm) and the gap between the two plates was set to 1.0 mm. Next, the temperature was increased from 25 to 85 °C at a rate of 2 °C/min, maintained at 85 °C for 15 min, and then decreased to 25 °C at a rate of 2 °C/min to obtain the changes in storage modulus (G′) and loss modulus (G″) of the samples during the temperature sweep. The emulsion gels were cooled to room temperature, the frequency was scanned at 25 °C, and the changes in G′ and G″ of the emulsion gels were obtained in the variation range 0.1–100 rad/s. In order to show the changes in the rheological behavior of the emulsion gels prepared with SPI and anionic polysaccharides, frequency sweep was also applied to the emulsions to determine their G′ and G″.

2.4.6. Oxidation resistance

For the determination of the antioxidant properties of the emulsion gels, the method of Flaiz et al. (2016) was slight modified. In brief, 7.0 mmol/L ABTS solution and 2.45 mmol/L potassium persulfate solution were prepared, both of which were mixed in equal volume ratios and diluted with methanol to certain concentrations for subsequent determination. Next, 0.1 mmol/L DPPH solution was prepared and diluted with methanol to certain concentrations, and 100 μL samples were placed into 10 ml centrifuge tubes and 5 ml of the above two solutions were added to each sample. The samples were incubated in a warm water bath for 30 min in darkness, the supernatant was obtained by centrifugation (4000 r/min, 10 min, 4 °C) after the end of the reaction, and the absorbance values of the supernatants were measured at 734 nm. The methanol solution served as the blank, and the free radical scavenging rate was calculated according to the following equation:

$$\mathrm{S}(\%) = \left(1 - \frac{\lambda \mathrm{S}}{\lambda \mathrm{c}}\right) \times 100\% \tag{4}$$

Where λ_S represents the absorbance of the sample, and λ_C represents the absorbance of the blank sample.

2.5. Digestion behavior

According to the method of Wei et al. (Wei & Huang, 2019), the gastrointestinal tract digestion model was constructed, simulated gastric fluids (SGF) and simulated intestinal fluids (SIF) were prepared, and the reaction temperature was controlled at 37 °C. According to previous results, CA2/GA2 and CA3/GA3 were selected for digestion characteristics analysis. SGF was comprised of 0.20% (*w/v*) NaCl, 0.70% (*v*/v) HCl, and 0.32% (w/v) pepsin solution. SIF was comprised of 0.70% (w/v) bile salt, 0.50% (w/v) trypsin, 0.40% (w/v) lipase, and 0.80% (w/v) $CaCl_2$ solution. 10 ml SGF was added to 10 ml the emulsion gel, followed by incubation on a shaking table for 2 h (200 r/min, 37 °C). During incubation, the pH of the reaction was maintained at 2.00 ± 0.02 with 0.1 M HCl. After incubation, the pH of the mixture was adjusted to 7.00 ± 0.02 to stop the digestion of gastric fluids. An equal volume of SIF was added to the reaction solution after gastric fluid digestion, followed by incubation on a shaking table for 2 h (200 r/min, 37 °C). During incubation, the pH of the reaction was maintained at 7.50 ± 0.02 with 1 M NaOH, and the amount of NaOH solution consumed was recorded. After digestion, the sample was immersed in ice water to stop the digestion of intestinal fluids.

2.5.1. Release rate of vitamin E

The method of Chen, Mao, Hou, Yuan, and Gao (2020) was slightly modified to determine the content of vitamin E in the digested emulsion gels. In brief, 5.0 ml of each digested sample was weighed and mixed

with 5.0 ml of ethanol to remove the released vitamin E from the emulsion gels. After centrifugation (3000 *g*, 15 min, 4 °C), 5 ml of n-hexane was added to the precipitate, and the samples were mixed and centrifuged (8000 *g*, 20 min, 4 °C). The absorbance of the supernatant was measured at 285 nm. The content of vitamin E was calculated in the supernatant according to the standard curve of vitamin E, and the release rate of vitamin E was calculated according to the following formula (Stone, Cheung, Chang, & Nickerson, 2013):

$$\text{Release rate of vitamin E}(\%) = \frac{C_0 - C_t}{C_0} \times 100\% \quad (5)$$

Where C_0 is the vitamin E content in the emulsion gel before digestion, and C_t is the vitamin E content remaining in the emulsion gel after digestion.

2.5.2. Microstructure after simulated digestion

After the dilution of the digested sample 100 times (*v*/v), the changes in the particles of the digested emulsion gels were observed under the BX53 optical microscope (Olympus, Tokyo, Japan).

2.5.3. Release of free fatty acids (FFAs)

The release of free fatty acids (FFAs) during digestion can be calculated according to the consumption of NaOH solution (Shi et al., 2021), and the release of FFA can indicate the extent of lipolysis of the samples. The release rate of FFA can be calculated according to the following formula:

$$\text{FFA}(\%) = \left(\frac{M_{oil} \times V_{NaOH} \times m_{NaOH}}{2 \times \omega_{oil}}\right) \times 100\% \quad (6)$$

Where M_{oil} is the molecular mass of oil (g/mol), V_{NaOH} is the volume of NaOH solution consumed when neutralizing the released FFA (L), M_{NaOH} is the concentration of NaOH solution (1 mol/L), and w_{oil} is the mass of oil in the emulsion gel before digestion (g).

2.5.4. Bioaccessibility

In brief, 10 mL digested samples were centrifuged for 20 min (4000 r/min, 25 °C), and 1 ml of the supernatant was mixed with 5 mL of the solvent (ethanol:n-hexane (*v*/v, 1:2)) and centrifuged (1000 r/min for 5 min). The absorbance of the supernatant was measured at 285 nm (Yan et al., 2020). The content of vitamin E was calculated according to the vitamin E standard curve. The bioaccessibility was calculated according to the following formula:

$$\text{Bioaccessibility} = \frac{C_1}{C_2} \times 100\% \quad (7)$$

Where C_1 is the concentration of vitamin E measured (mg/g), and C_2 is the total concentration of vitamin E (mg/g).

2.6. Statistical analysis

Each experiment was repeated three times. The statistical significance of the results was tested by SPSS, and the difference between the mean values of each group was analyzed by LSD multi range test with a probability level of 0.05 ($p < 0.05$).

3. Results and discussion

3.1. SPI-CA/GA complex characterization

3.1.1. Fourier transform infrared spectroscopy (FT-IR)

Protein has a characteristic absorption band in the infrared region, which can reflect changes in the functional groups of the protein (Liang et al., 2020). When both SPI and anionic polysaccharides have net negative charge, they generally tended to form soluble SPI-CA/GA complexes, where the attraction between SPI and anionic polysaccharides was caused by the positive charge regions of SPI interacting with CA and GA (Han, Zhu, Zhang, Liu, & Wu, 2024). As shown in Fig. 1 A and B, except for the characteristic absorption peak of sulfuric acid group of CA in the 840–930 cm^{-1} wavelength range (Gomez-Ordonez & Ruperez, 2011), no new absorption peak appeared in the spectra of the SPI-CA/GA complex compared to SPI, indicating that the addition of CA and GA did not cause the formation of a new substance. After the addition of CA and GA, the peak value and peak width of the 3292 cm^{-1} wave segment in the amide A band (3100–3500 cm^{-1}) changed slightly, which may be due to the condensation of SPI and anionic polysaccharides to produce the hydrogen bond (C. Zhang et al., 2020). Furthermore, in order to obtain information concerning the amide I band (1600–1700 cm^{-1}) changes, the amide I region was investigated as second derivative spectra and the proportions of α-helix, β-sheet, β-turn and random coil are calculated in Fig. 1 A1 and B1. With the increasing of CA and GA concentration, the content of α-helix and random coil first decreased and then increased, while the content of β-sheet and β-turn first increased and then decreased. In terms of the structure of the protein, β-sheet and β-turn were related to hydrogen bonds. Therefore, an increase in the number of β-sheet and β-turn indicated that there were hydrogen bonds between SPI and anionic polysaccharides, and they could combine to form complexes through electrostatic interactions (Li et al., 2019).

3.1.2. Intrinsic fluorescence spectrum

Intrinsic fluorescence spectra can be used to reflect the changes of protein structure. When the excitation wavelength is 295 nm, the change in the fluorescence spectrum is mainly caused by the change of tryptophan (Trp) residues. As shown in Fig. 1 C, with the increasing of CA and GA concentrations, the maximum emission peak intensity of SPI decreased, but the shape of the peak remained unchanged, showing a typical fluorescence quenching phenomenon, indicating that there was an interaction between anionic polysaccharides and SPI. In addition, the maximum emission wavelength of SPI had a slight blue shift, which indicated that SPI and anionic polysaccharides had combined to form a complex (Ma et al., 2020). The addition of CA and GA increased the space steric resistance between SPI particles, which leaded to the transformation of SPI secondary structures, exposure of hydrophobic groups in SPI, and reduced the fluorescence intensity. The internal microenvironment of Trp had a trend of change from polar to non-polar, which resulted in the blue shift of the maximum absorption wavelength of Trp.

3.1.3. Particle size and zeta potential

The average particle size and the particle size distribution of SPI-CA and SPI-GA complexes are shown in Fig. 1 D. The particle sizes of the complexes first decreased and then increased after CA and GA were added. When the particle sizes of the complexes decreased with the increase of the CA and GA concentration, it showed that the addition of CA and GA broke the aggregation of SPI particles, making the distribution of particles more uniform. Furthermore, the particle sizes of SPI-CA and SPI-GA was smaller, which indicated that the complexes were more stable. However, when the anionic polysaccharides were excessive (CA4/GA4), a large number of CA and GA gathered around SPI particles or the aggregation of SPI, so the particle sizes of the complexes were increased, and the stabilities of the complexes were decreased.

Fig. 1 D show that the Zeta potential value of the complexes increased significantly ($p < 0.05$) after the addition of CA and GA. The sulfur group on the CA side chain and the carboxyl group on the GA side chain carried negative charges, and SPI carried negative charges. Therefore, the aggregation between SPI particles was destroyed by electrostatic repulsion, and amino groups and carboxyl groups of the SPI structure were exposed. Furthermore, CA and GA adsorbed with the amino groups of SPI to form neutral complexes, resulting in increasing of the absolute value of the potential (Stone et al., 2013). Compared to GA, CA could make the expansion of SPI better, expose more amino groups, and have a better binding effect with SPI in a certain concentration.

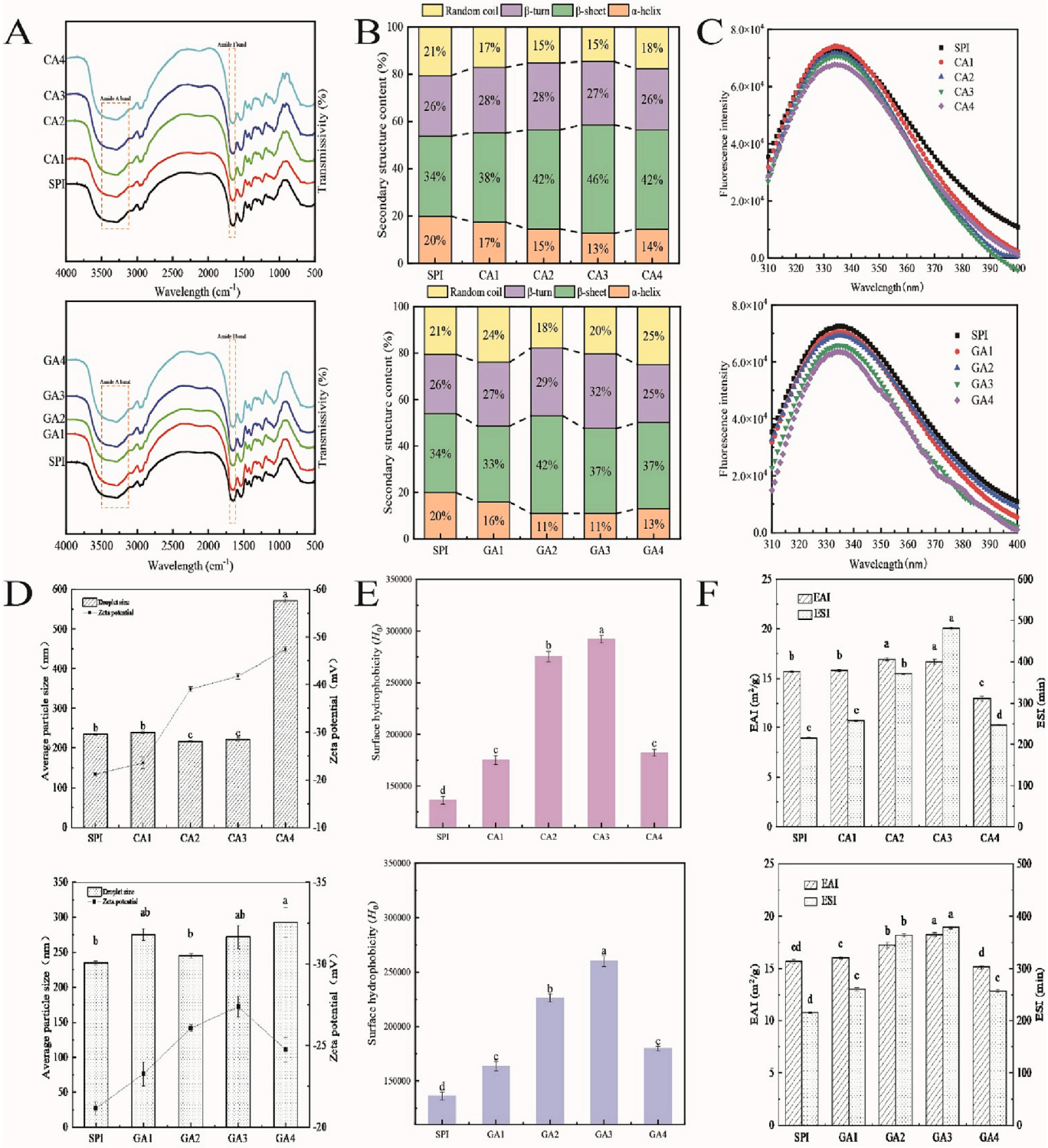

Fig. 1. FT-IR (A), secondary structure analysis (B), intrinsic fluorescence spectra (C), average particle size and Zeta potential (D), surface hydrophobicity (E), ESI and EAI (F) of the complexes with different anionic polysaccharides concentration.

However, because of the large charge density of CA, when more CA was added, surplus CA in the system failed to combine with SPI, so the Zeta potential of the system still showed an increasing trend.

3.1.4. *Surface hydrophobicity(H_0)*

The surface hydrophobicity (H_0) of protein is closely related to its emulsifying ability and stability (X. M. Liu, Powers, Swanson, Hill, & Clark, 2005). As shown in Fig. 1 E, with increasing of CA and GA concentrations, the surface hydrophobicity of SPI significantly ($p < 0.05$) increased and then decreased. This indicated that the addition of polysaccharides changed the microenvironment of SPI, and the molecular structure of SPI expanded to expose more hydrophobic groups that could combine with the ANS probe. When the concentration exceeded 0.10% (>CA3/GA3), the H_0 of SPI decreased. This may be because the content of CA and GA increased, the hydrophobic groups of the unfolded structure were wrapped in the system again by the viscosity of the

system or the aggregation between particles, resulting in the decreased H_0 of the system (Ren et al., 2020). Compared to GA, the presence of CA was more conducive to the expansion of the SPI structure and the exposure of hydrophobic groups.

3.1.5. Emulsification properties

As shown in Fig. 1 F, with the increase of CA and GA concentrations, the EAI and the ESI of the emulsions first increased and then decreased. The addition of CA and GA contributed to the exposure of more hydrophobic groups, and enhanced interaction between protein and oil droplets, resulting in the increase of EAI. Furthermore, the addition of CA and GA enhanced the steric resistance between particles, the electrostatic repulsion, and prevented the flocculation of droplets, resulting in improving the ESI of the emulsions (T. Yang, Li, & Tang, 2020). GA contains a small amount of protein, which contributes to the adsorption of SPI at the oil-water interface, making it conducive to improved emulsification activity. However, excessive CA and GA might have a shielding effect on SPI to reduce the amount of SPI adsorbed at the oil/water interface, resulting in the decrease of EAI and ESI.

3.2. SPI-CA/GA emulsion gel characterization

3.2.1. Microstructure

The properties of the emulsion gel are related to its network structure. The microstructure images of SPI-CA/GA emulsion gels are shown in Fig. 2. All samples could form continuous three-dimensional network structures. SPI-CA/GA emulsions due to heating treatment and Ca^{2+} made the interaction between SPI through inter-chain and intra-chain disulfide bonds, thus forming the spatial network structure, and the interaction between Ca^{2+} and SPI effective action sites was enhanced, so that more oil droplets entered into the network structure, thus enhancing the strength of the emulsion gel (Spotti, Tarhan, Schaffter, Corvalan, & Campanella, 2017). With the increase of the CA concentration in the system, the porosity of the emulsion decreased, and the structure became more uniform and continuous, and dominated by a lamellar structure. The oil droplets also polymerized with oil droplets and were embedded in the network structure, which indicated SPI-CA emulsion gel can be classified as an emulsion-filled gel. With the increase of the GA concentration, the aggregation of oil droplets in the emulsion gel increased, and the oil droplets floated on the network structure. The structure of SPI-GA emulsion gel was dominated by the interaction between oil droplets, supplemented by the continuous network structure of the proteins. In the SPI-GA emulsion gel structure, oil droplets gathered to form a network structure, which indicated SPI-GA emulsion gel can be classified as an emulsion-aggregated gels. In summary, it indicated that the oil droplets in SPI-CA emulsion gels were dispersed in a continuous gel network formed by cross-linking of proteins, whereas the oil droplets in SPI-GA emulsion gels were dispersed in a gel network formed by oil droplets through flocculation. However, when the concentrations of CA and GA were excessive (CA4/GA4), the structure of the emulsion gels became loose, with larger pores and increased porosity.

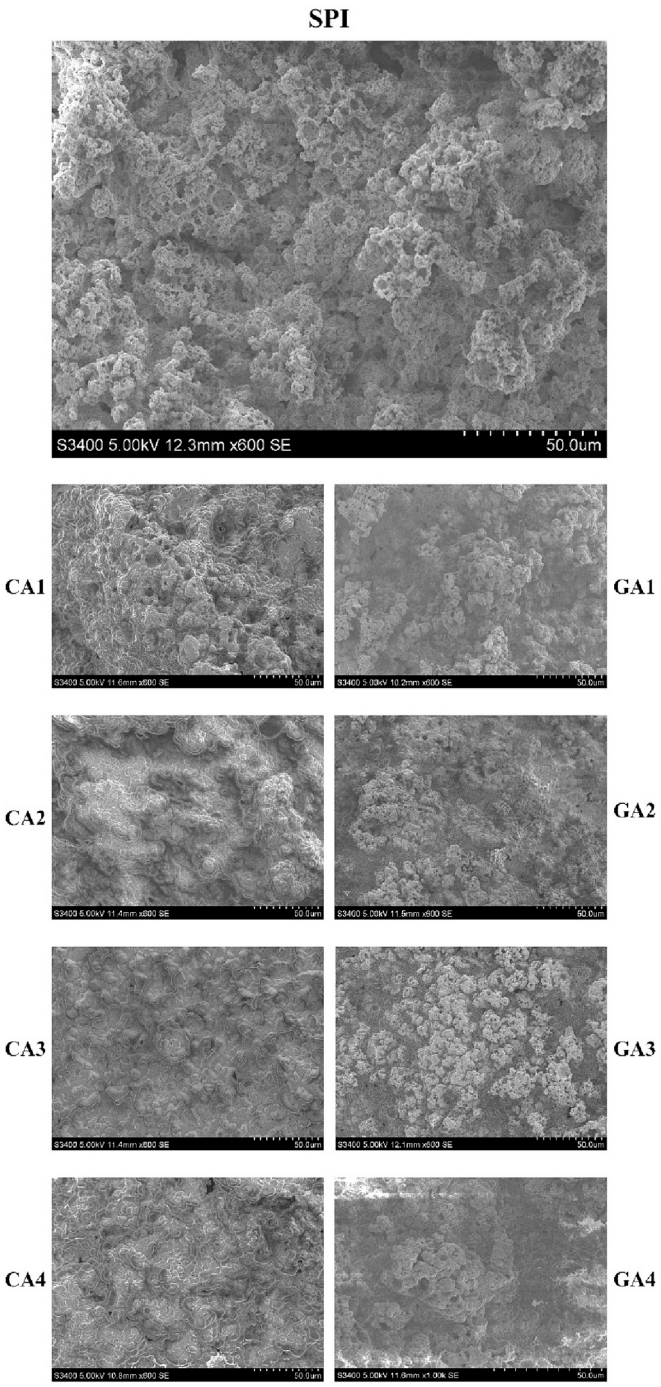

Fig. 2. Microstructure images of the emulsion gels with different anionic polysaccharides concentration.

3.2.2. Force of emulsion gels

The forces in the emulsion gel network structure are shown in Fig. 3 A. The main forces for the formation of the network structure of the SPI emulsion gel were ionic bond and disulfide bond, accounting for >65% of total bonds, while the hydrogen bond and hydrophobic interaction accounted for <30% of total bonds. With the increase of CA and GA concentrations, the ionic bond decreased, and the disulfide bonds first decreased and then increased. After the addition of CA and GA, the number of hydrogen bonds significantly ($p < 0.05$) increased, which may be due to the negative charges of CA and GA that could break up the aggregation between SPI particles and reduced the particle size of the SPI molecules, thus enhancing the electrostatic interaction between proteins (X. Yang, Su, & Li, 2020). Furthermore, the addition of CA and GA increased the exposure of SPI hydrophobic groups, resulting in the increase of hydrophobic interactions between proteins and proteins with increasing CA and GA concentrations.

3.2.3. Water holding capacity (WHC)

The water-holding capacity of a gel is an important property of foods, and it has an important impact on food quality (Wang et al., 2018). It can be seen from Fig. 3 B that with the increase of CA and GA concentrations, the WHC of the emulsion gels gradually increased and then decreased. The combination of SPI and anionic polysaccharides enhanced the interaction between the emulsion gel matrix, forming stronger capillaries, and the gel network became more detailed and uniform, thus

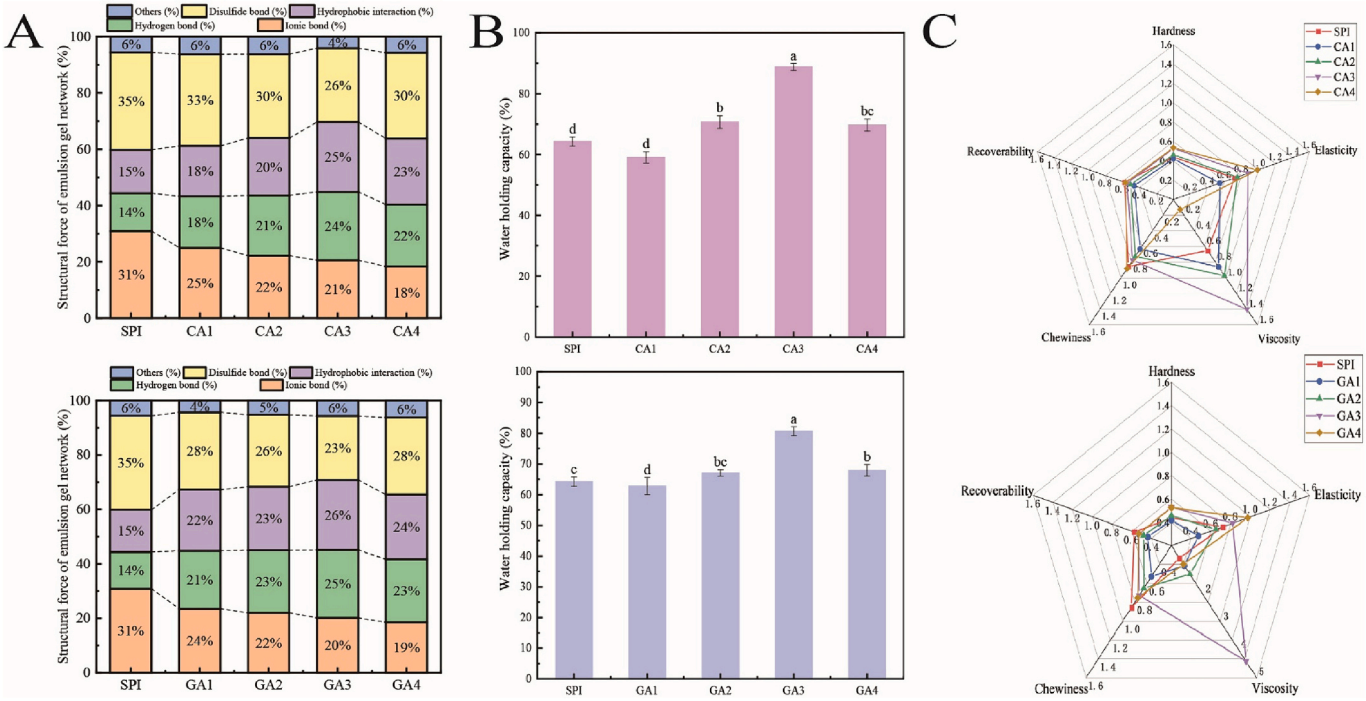

Fig. 3. Structural force (A), water holding capacity (B), and texture characteristics (C) of the emulsion gels with different anionic polysaccharides concentration.

enhancing the gel strength of the gels, so as to retain more water and to enhance the water retention of the emulsion gel (Lv et al., 2020). However, when the emulsion gel was CA4/GA4, the emulsion gels with large pores or coarse structures had poor WHC due to weak capillaries. When CA and GA concentrations were higher than 0.01% (>CA1/GA1), the WHC of SPI-CA emulsion gel was better than that of SPI-GA emulsion gel, indicating that the structure of SPI-CA emulsion gel was more uniform, and the gel strength was better, so it could retain more water.

3.2.4. *Texture properties*

As shown in Fig. 3 C, the hardness of the samples was <1, indicating that the emulsion gels in this study were soft gels and the hardness was not significantly ($P < 0.05$) different across the gels. The elasticity of the emulsion gels increased significantly ($P < 0.05$) with the increase of CA and GA concentrations, indicating that the addition of CA and GA changed the surface hydrophobicity of SPI, improved the interactions between oil droplets, and improved the three-dimensional network structure of the emulsion gels. Compared with the GA emulsion gel, the CA emulsion gel had slightly higher elasticity. With the increase of CA and GA concentrations, the viscosity of the emulsion gels first increased and then decreased. The viscosity of the SPI emulsion gel was 0.652. After the addition of anionic polysaccharides, the viscosity increased significantly ($P < 0.05$) to 1.402 (CA3) and 4.401 (GA3). The viscosity of the SPI-GA emulsion gel was higher than that of the SPI-CA emulsion gel. GA might tend to increase the viscosity of the emulsion and emulsion gel. The results of chewiness and recoverability were the same as that of elasticity. Elasticity played an important role in the chewiness and recoverability of the gels. The emulsion gels with better elasticity also

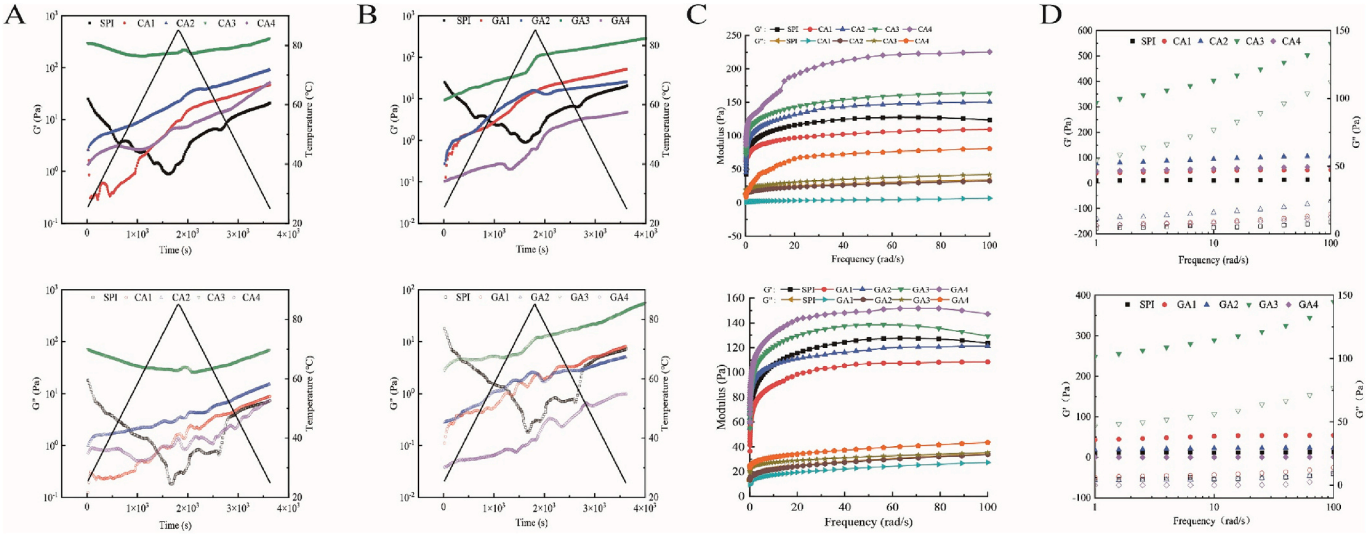

Fig. 4. Temperature sweep (A, B) of emulsion gels, frequency sweep of the emulsions (C) and the emulsion gels (D) with different anionic polysaccharides concentration.

had better molding effects, and emulsion gels prepared by CA had better formability, and the force required to form the gel network structure was stronger. CA emulsion gels are suitable for the application of products with more compressibility, recoverability, high elasticity, and low viscosity.

3.2.5. Rheological behavior

3.2.5.1. Temperature sweep. As shown in Fig. 4 A and B, there is no crossover between G′ and G″ suggesting no gel formation transition and formed network from the start of the measurement, indicating that all emulsion gels were elastic, and formed three-dimensional network structures. In the heating stage, the G′ and G″ of the SPI-CA emulsion gels increased with the increase of temperature (except CA3). When the temperature reached 40–60 °C, the modulus of the SPI-CA emulsion gels continued to increase and exceeded that of the SPI emulsion gel, indicating that CA was beneficial to the formation of the emulsion gel network structure, increased the elasticity of the emulsion gel and rendered the network structure more compact (Luo, Ye, Wolber, & Singh, 2019). In the heating stage, G′ and G″ of the SPI-GA emulsion gel increased with increasing temperature. When the temperature changed from 30 to 55 °C, the modulus of the GA emulsion gel began to be larger than that of the SPI emulsion gel. However, when the emulsion gels were CA4 and GA4, the modulus of the emulsion gel decreased and was lower than that of the SPI emulsion gel, indicating that the gel properties were weakened, and the force between gel networks was weakened. Furthermore, the modulus of CA3 emulsion gel return to the initial modulus, indicating that the CA3 emulsion gel have thermal reversibility.

3.2.5.2. Frequency sweep. For the emulsions, as shown in Fig. 4 C. With the increase of shear frequency, the shear modulus of the emulsions increased rapidly, and then tended to stabilize. The G′ was significantly greater than G″, indicating that all emulsions were elastic. Furthermore, the G′ and G″ of the SPI-CA emulsion was greater than that of the SPI-GA emulsion. Compared with GA emulsion, the CA emulsion had higher modulus and better elastic properties.

As shown in Fig. 4 D, the G′ of all samples was greater than G″, indicating that emulsions formed three-dimensional network structures through interactions between droplets and between continuous phases of SPI and polysaccharides during gelation, which prompted emulsions to form emulsion gels with elastic properties (S. Li, Zhang, Li, Fu, & Huang, 2020). With the increase of CA and GA concentrations, the modulus of the emulsion gels gradually increased in the frequency range. However, when the emulsion gel was CA4/GA4, the modulus of the emulsion gels decreased, even lower than that of the SPI emulsion gel, indicating that the addition of an appropriate amount of CA and GA helped to promote the formation of the gel network structure and enhanced the interaction between emulsion gels. The addition of excessive CA and GA reduced the interaction between the emulsion oil drops and the complexes and rendered the network structure loose. Besides, compared with the emulsions, the G′ and G″ of the all emulsion gels was greater, which indicated that the emulsion gels had higher elasticity, formed denser network structure, and thus had better applicability.

3.2.6. Oxidation resistance

The antioxidant activity test results of the SPI-CA and SPI-GA emulsion gels are shown in Fig. 5. The antioxidant activities of the emulsion gels were evaluated by their scavenging ability in DPPH and ABTS free radicals. The addition of CA and GA significantly ($p < 0.05$) improved the free radical scavenging capacities of the emulsion gels. Within a certain range, the higher concentration of CA and GA, the stronger the antioxidant capacity of the emulsion gels. This may be because the increase in hydrogen bonds after the addition of CA and GA, which can quench radicals, and hydrogen bonds could promote hydrogen abstraction and proton dissociation reactions of hydroxyl groups. In addition, due to the presence of reductones in CA and GA, they could react with certain peroxide precursors to prevent the formation of peroxides, resulting in improving antioxidant capacity of the emulsion gels.

3.3. Digestive characteristics

3.3.1. Release rate of vitamin E

The release rates of vitamin E during emulsion gel digestion are shown in Fig. 6 A. The addition of CA and GA decreased the release rate of vitamin E in the emulsion gels with the increase of CA and GA concentrations. With the increase of the concentration, the release rate of vitamin E decreased during digestion, indicating that after the addition of CA and GA, emulsion gels formed a denser interfacial film on the surface of the oil phase that could effectively prevent the release of vitamin E. Besides, the anti-digestion abilities of the emulsion gels were enhanced, which slowed down the hydrolysis of the enzymes, and the release of vitamin E was reduced.

3.3.2. Microstructure after simulated digestion

The dispersion of gel particles after the digestion of emulsion gels was observed with an optical microscope. The results are shown in Fig. 6 D. After digestion of simulated gastric fluids, the emulsion gel particles became larger and had a small amount of flocculation, which indicated that proteins started to be hydrolyzed under the action of pepsin, and oil droplets slowly became larger. After the digestion of the simulated intestinal fluid, all emulsion gel particles of SPI-CA aggregated, revealing

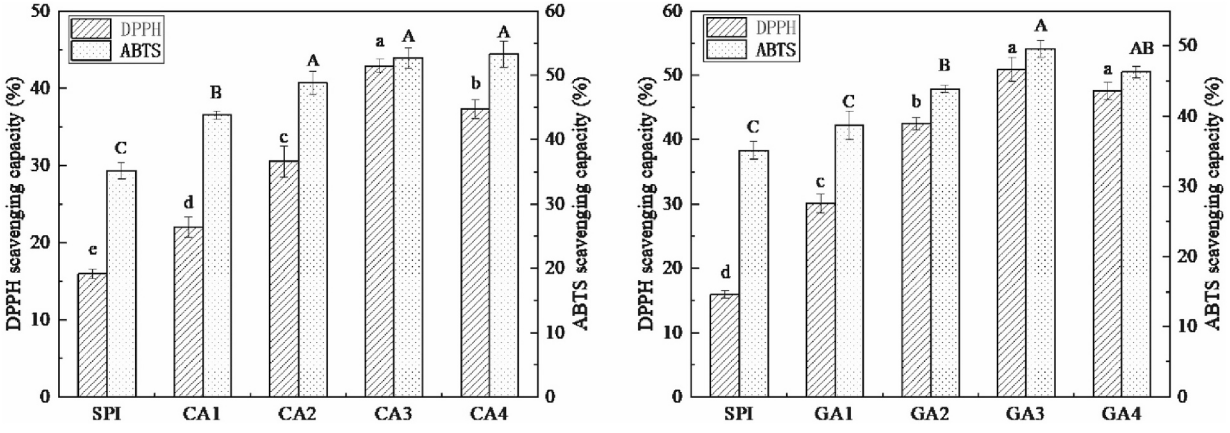

Fig. 5. Antioxidant activity of the emulsion gels with different anionic polysaccharides concentration.

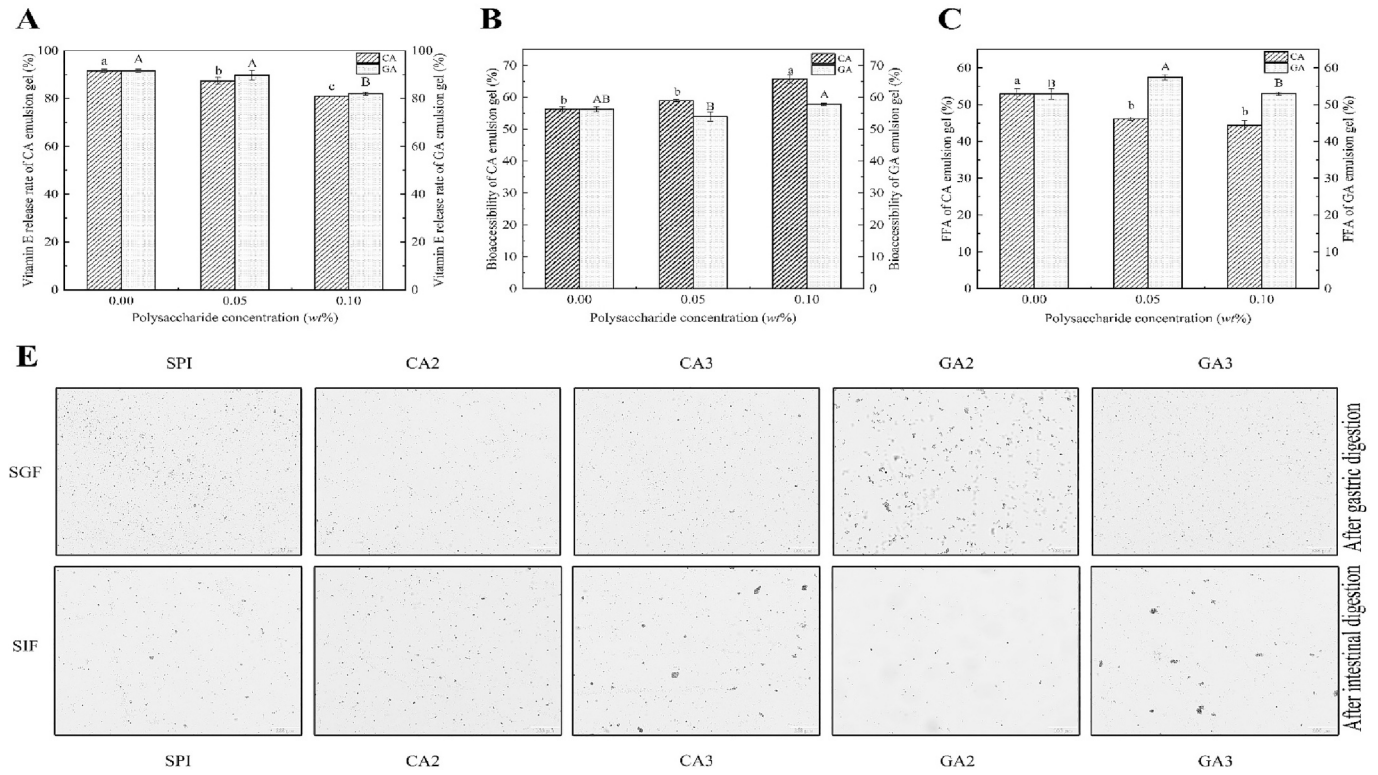

Fig. 6. Release rate of vitamin E (A), release of free fatty acids (B), bioaccessibility (C), and microstructure of the emulsion gels (D) with different anionic polysaccharides concentration after digestion.

that the gel structure was destroyed, the oil in the gel network structure was released. For the SPI-GA emulsion gel, when the emulsion gel was GA2, the gel particles gathered, and the particle size was much larger than that of the SPI emulsion gel, indicating that the protective effect of the emulsion gel on lipid digestion was not good during digestion of simulated gastric fluid.

3.3.3. Release of free fatty acids (FFAs)

As shown in Fig. 6 B, the addition of CA significantly ($P < 0.05$) reduced the FFA release rate of the emulsion gel from 52.9% to 44.49%, while the addition of GA increased the FFA release rate of the emulsion gel from 52.9% to 57.4%. This difference may be related to the network structure of the emulsion gels. The microstructure of the SPI-CA emulsion gel showed that the gel network structure was dense, and the oil droplets were wrapped in the network structure, thus slowing down the release of FFAs. However, the SPI-GA emulsion gel network structure was "semi suspended", and the oil drops were suspended outside the gel, which promoted the digestion of lipids. With the increase of the GA concentration, the viscosity of the emulsion gel increased, and the relative movement between the oil droplets decreased, which reduced the hydrolysis of lipase, so the digestibility of lipids decreased.

3.3.4. Bioaccessibility

As shown in Fig. 6 C, the bioaccessibility of SPI-CA emulsion gel increased significantly ($P < 0.05$) with the increase of CA concentration, which indicated that the addition of CA effectively protected vitamin E, and the emulsion gel prepared from SPI-CA complexes are capable of slow and targeted release of vitamin E. Because the particles of CA increased slightly, the small oil droplets were digested faster, and they had a larger specific surface area, which resulted in higher bioavailability since more vitamin E could be retained in the micelles. However, the bioaccessibility of SPI-GA emulsion gel increased slightly with the increase of the GA concentration, which indicated that the aggregation of the SPI-GA emulsion gel particles and its gel structure were not good for protecting vitamin E to reach intestinal digestion.

4. Conclusion

In this study, the effect of CA and GA on SPI structure was investigated by characterizing the complexes and the emulsion gels. SPI-CA and SPI-GA complexes were more stable, and had greater emulsification properties, and were conducive to the preparation of the emulsion gels. SPI-CA and SPI-GA emulsion gels had good WHC and oxidation resistances. CA formed emulsion-filled gels with good elasticity and thermal reversibility, whereas GA formed an emulsion-aggregated gel with good viscosity. Both could slow down the vitamin E digestion and release rate in gastric digestion, but CA had a better protective effect. In summary, both CA and GA could form complexes with SPI through non-covalent interactions and improve the functional properties of emulsion gels, effectively protect fat-soluble nutrients and realize targeted slow release, which is an excellent delivery system for fat-soluble nutrients. This study is expected to provide a theoretical basis for exploring the interaction between anionic polysaccharide and SPI, and a foundation of the preparation and development of SPI-anionic polysaccharide emulsion gel.

CRediT authorship contribution statement

Tian Gao: Writing – review & editing, Writing – original draft, Visualization, Methodology, Formal analysis, Conceptualization. **Xixi Wu:** Software, Resources, Data curation. **Yiting Gao:** Validation, Investigation, Formal analysis. **Fei Teng:** Supervision, Funding acquisition, Formal analysis. **Yang Li:** Project administration, Formal analysis.

Declaration of competing interest

To the best of our knowledge, the named authors have no conflict of

interest, financial or otherwise.

Data availability

The data that has been used is confidential.

Acknowledgments

This work was funded by the Natural Science Foundation of China (No.32001686), the Natural Science Foundation of Heilongjiang Province of China (No.LH2020C028).

References

Chen, C., Sun-Waterhouse, D., Zhang, Y., Zhao, M., & Sun, W. (2020). The chemistry behind the antioxidant actions of soy protein isolate hydrolysates in a liposomal system: Their performance in aqueous solutions and liposomes. *Food Chemistry, 323*.

Chen, H., Mao, L., Hou, Z., Yuan, F., & Gao, Y. (2020). Roles of additional emulsifiers in the structures of emulsion gels and stability of vitamin E. *Food Hydrocolloids, 99*.

Flaiz, L., Freire, M., Cofrades, S., Mateos, R., Weiss, J., Jimenez-Colmenero, F., & Bou, R. (2016). Comparison of simple, double and gelled double emulsions as hydroxytyrosol and n-3 fatty acid delivery systems. *Food Chemistry, 213*, 49–57.

Gali, L., Bedjou, F., Ferrari, G., & Donsi, F. (2022). Formulation and characterization of zein/gum arabic nanoparticles for the encapsulation of a rutin-rich extract from Ruta chalepensis L. *Food Chemistry, 367*.

Gomez-Ordonez, E., & Ruperez, P. (2011). FTIR-ATR spectroscopy as a tool for polysaccharide identification in edible brown and red seaweeds. *Food Hydrocolloids, 25*(6), 1514–1520.

Guo, Z., Wei, Y., Zhang, Y., Xu, Y., Zheng, L., Zhu, B., & Yao, Z. (2022). Carrageenan oligosaccharides: A comprehensive review of preparation, isolation, purification, structure, biological activities and applications. *Algal Research-Biomass Biofuels and Bioproducts, 61*.

Han, Y., Zhu, L., Zhang, H., Liu, T., & Wu, G. (2024). Characteristic of the interaction mechanism between soy protein isolate and functional polysaccharide with different charge characteristics and exploration of the foaming properties. *Food Hydrocolloids, 150*, Article 109615.

Khalesi, H., Emadzadeh, B., Kadkhodaee, R., & Fang, Y. (2019). Effect of Persian gum on whey protein concentrate cold-set emulsion gel: Structure and rheology study. *International Journal of Biological Macromolecules, 125*, 17–26.

Kornet, R., Sridharan, S., Venema, P., Sagis, L. M. C., Nikiforidis, C. V., van der Goot, A. J., … van der Linden, E. (2022). Fractionation methods affect the gelling properties of pea proteins in emulsion-filled gels. *Food Hydrocolloids, 125*.

Lee, H., Yildiz, G., dos Santos, L. C., Jiang, S., Andrade, J. E., Engeseth, N. J., & Feng, H. (2016). Soy protein nano-aggregates with improved functional properties prepared by sequential pH treatment and ultrasonication. *Food Hydrocolloids, 55*, 200–209.

Li, H., Liu, T., Zou, X., Yang, C., Li, H., Cui, W., & Yu, J. (2021). Utilization of thermal-denatured whey protein isolate-milk fat emulsion gel microparticles as stabilizers and fat replacers in low-fat yogurt. *LWT- Food Science and Technology, 150*.

Li, L., He, M., Yang, H., Wang, N., Kong, Y., Li, Y., & Teng, F. (2021). Effect of soybean lipophilic protein-methyl cellulose complex on the stability and digestive properties of water-in-oil-in-water emulsion containing vitamin B-12. *Colloids and Surfaces A: Physicochemical and Engineering Aspects, 629*.

Li, Q., Wang, Z., Dai, C., Wang, Y., Chen, W., Ju, X., … He, R. (2019). Physical stability and microstructure of rapeseed protein isolate/gum Arabic stabilized emulsions at alkaline pH. *Food Hydrocolloids, 88*, 50–57.

Li, Q., Zheng, J., Ge, G., Zhao, M., & Sun, W. (2020). Impact of heating treatments on physical stability and lipid-protein co-oxidation in oil-in-water emulsion prepared with soy protein isolates. *Food Hydrocolloids, 100*.

Li, S., Zhang, B., Li, C., Fu, X., & Huang, Q. (2020). Pickering emulsion gel stabilized by octenylsuccinate quinoa starch granule as lutein carrier: Role of the gel network. *Food Chemistry, 305*.

Liang, X., Ma, C., Yan, X., Zeng, H., McClements, D. J., Liu, X., & Liu, F. (2020). Structure, rheology and functionality of whey protein emulsion gels: Effects of double cross-linking with transglutaminase and calcium ions. *Food Hydrocolloids, 102*.

Liu, S., Zhao, M., Hu, K., & Lin, W. (2003). Effects of k-carrageenan on characteristics of soy protein isolate emulsion gels. *Food and Fermentation Industries, 29*(11), 10–13.

Liu, X. M., Powers, J. R., Swanson, B. G., Hill, H. H., & Clark, S. (2005). Modification of whey protein concentrate hydrophobicity by high hydrostatic pressure. *Innovative Food Science & Emerging Technologies, 6*(3), 310–317.

Lopes-da-Silva, J. A., & Monteiro, S. R. (2019). Gelling and emulsifying properties of soy protein hydrolysates in the presence of a neutral polysaccharide. *Food Chemistry, 294*, 216–223.

Loyeau, P. A., Spotti, M. J., Vinderola, G., & Carrara, C. R. (2021). Encapsulation of potential probiotic and canola oil through emulsification and ionotropic gelation, using protein/polysaccharides Maillard conjugates as emulsifiers. *LWT-Food Science And Technology, 150*.

Luo, N., Ye, A., Wolber, F. M., & Singh, H. (2019). Structure of whey protein emulsion gels containing capsaicinoids: Impact on in-mouth breakdown behaviour and sensory perception. *Food Hydrocolloids, 92*, 19–29.

Lv, P., Wang, D., Chen, Y., Zhu, S., Zhang, J., Mao, L., … Yuan, F. (2020). Pickering emulsion gels stabilized by novel complex particles of high-pressure-induced WPI gel and chitosan: Fabrication, characterization and encapsulation. *Food Hydrocolloids, 108*.

Ma, X., Hou, F., Zhao, H., Wang, D., Chen, W., Miao, S., & Liu, D. (2020). Conjugation of soy protein isolate (SPI) with pectin by ultrasound treatment. *Food Hydrocolloids, 108*.

Maltais, A., Remondetto, G. E., Gonzalez, R., & Subirade, M. (2005). Formation of soy protein isolate cold-set gels: Protein and salt effects. *Journal of Food Science, 70*(1), C67–C73.

Puppo, M. C., Beaumal, V., Chapleau, N., Speroni, F., de Lamballeriec, M., Anon, M. C., & Anton, M. (2008). Physicochemical and rheological properties of soybean protein emulsions processed with a combined temperature/high-pressure treatment. *Food Hydrocolloids, 22*(6), 1079–1089.

Ren, S., Liu, L., Li, Y., Qian, H., Tong, L., Wang, L., Zhou, X., Wang, L., & Zhou, S. (2020). Effects of carboxymethylcellulose and soybean soluble polysaccharides on the stability of mung bean protein isolates in aqueous solution. *LWT- Food Science and Technology, 132*.

Shi, F., Tian, X., McClements, D. J., Chang, Y., Shen, J., & Xue, C. (2021). Influence of molecular weight of an anionic marine polysaccharide (sulfated fucan) on the stability and digestibility of multilayer emulsions: Establishment of structure-function relationships. *Food Hydrocolloids, 113*.

Spotti, M. J., Tarhan, Ö., Schaffter, S., Corvalan, C., & Campanella, O. H. (2017). Whey protein gelation induced by enzymatic hydrolysis and heat treatment: Comparison of creep and recovery behavior. *Food Hydrocolloids, 63*, 696–704.

Stone, A. K., Cheung, L., Chang, C., & Nickerson, M. T. (2013). Formation and functionality of soluble and insoluble electrostatic complexes within mixtures of canola protein isolate and (kappa-, iota- and lambda-type) carrageenan. *Food Research International, 54*(1), 195–202.

Wang, X., Zeng, M., Qin, F., Adhikari, B., He, Z., & Chen, J. (2018). Enhanced CaSO4-induced gelation properties of soy protein isolate emulsion by pre-aggregation. *Food Chemistry, 242*, 459–465.

Wei, Z., & Huang, Q. (2019). Developing organogel-based Pickering emulsions with improved freeze-thaw stability and hesperidin bioaccessibility. *Food Hydrocolloids, 93*, 68–77.

Yan, Y., Zhu, Q., Diao, C., Wang, J., Wu, Z., & Wang, H. (2020). Enhanced physicochemical stability of lutein-enriched emulsions by polyphenol-protein-polysaccharide conjugates and fat-soluble antioxidant. *Food Hydrocolloids, 101*.

Yang, T., Li, X.-T., & Tang, C.-H. (2020). Novel edible Pickering high-internal-phase-emulsion gels efficiently stabilized by unique polysaccharide-protein hybrid nanoparticles from Okara. *Food Hydrocolloids, 98*.

Yang, X., Su, Y., & Li, L. (2020). Study of soybean gel induced by *Lactobacillus plantarum*: Protein structure and intermolecular interaction. *LWT- Food Science and Technology, 119*.

Zhang, C., Li, Y., Wang, P., Li, J., Weiss, J., & Zhang, H. (2020). Core-shell nanofibers electrospun from O/W emulsions stabilized by the mixed monolayer of gelatin-gum Arabic complexes. *Food Hydrocolloids, 107*.

Zhang, Z., Chen, W., Zhou, X., Deng, Q., Dong, X., Yang, C., & Huang, F. (2021). Astaxanthin-loaded emulsion gels stabilized by Maillard reaction products of whey protein and flaxseed gum: Physicochemical characterization and in vitro digestibility. *Food Research International, 144*.

Zhao, R., Fu, W., Chen, Y., Li, B., Liu, S., & Li, Y. (2022). Structural modification of whey protein isolate by cinnamaldehyde and stabilization effect on beta-carotene-loaded emulsions and emulsion gels. *Food Chemistry, 366*.